Methodology of Detection and Classification of Selected Aviation Obstacles Based on UAV Dense Image Matching

Marta Lalak and Damian Wierzbicki

***Abstract*—Currently, more and more accurate data provided by UAVs make it possible to analyze land cover, which requires the detection of objects and their individual elements. Object detection and determination of their geometric features is possible thanks to dense point clouds generated based on imagery obtained from low altitudes. 3D data from UAVs turn out to be extremely useful for ensuring safety in the airspace in the close vicinity of the airport. This article presents the methodology of automatic aviation obstacle detection based on low altitude data (UAV). The research was carried out on a dense 3D point cloud. The developed methodology for detecting aviation obstacles consists of three main stages. The first is point cloud filtration based on height–preliminary identification of aviation obstacles, followed by 3D point cloud segmentation using a modified RANSAC algorithm, supplemented with two-dimensional vector data of aviation obstacles to improve the accuracy of the segmentation process. The last stage is the classification of aviation obstacles according to the adopted height and cross-section criterion. The proposed method of detecting aviation obstacles is characterized by high accuracy. The mean error of fitting the point cloud to the obstacle database ranged from $\pm$ 0.04 m to $\pm$ 0.07 m.**

***Index Terms*—Accuracy, air traffic control, image processing, remote sensing, unmanned aerial vehicles (UAVs).**

I. Introduction

OVER the past decade, the cost of using unmanned aerial vehicles (UAVs) in photogrammetric and remote sensing applications has been increasingly low. UAV are a cheap and effective alternative to obtaining data with the methods of classical aerial photogrammetry. Until recently, airborne laser scanning dominated the acquisition of spatial data. However, for several years there has been increasing use of UAVs to analyze 3-D objects using point clouds [1]. Thanks to easy and universal data acquisition and processing, the low-altitude technology is gaining an advantage over the previously used aerial photogrammetry.

Manuscript received October 17, 2021; revised January 8, 2022; accepted January 30, 2022. Date of publication February 7, 2022; date of current version February 24, 2022. This work was supported by the Military University of Technology in Warsaw and co-funded by the Military University of Aviation in Dęblin, Poland. *(Corresponding author: Damian Wierzbicki.)*

Marta Lalak is with the Institute of Navigation, Polish Air Force University, 08-521 Dęblin, Poland (e-mail: m.lalak@law.mil.pl).

Damian Wierzbicki is with the Department of Imagery Intelligence, Faculty of Civil Engineering and Geodesy, Military University of Technology, 00-908 Warsaw, Poland (e-mail: damian.wierzbicki@wat.edu.pl).

Digital Object Identifier 10.1109/JSTARS.2022.3149105

Automatic detection and recognition of individual objects and distinguishing their elements is critical for many applications, including damage assessment and all research related to these objects. One of such applications may also be the retrieval of information about aviation obstacles. Aviation obstacles with their location and dimensions, especially height, may endanger aircraft. First of all, it is essential during the aircraft's take-off and landing maneuvers. An unidentified obstacle may turn out to be a significant threat during critical phases of flight. As the detection of aviation obstacles is extremely important for the safety of aircraft in the airspace, The International Civil Aviation Organization (ICAO) introduced a series of planes to limit obstacles in order to ensure the safety of aircraft [2]. Objects that penetrate these planes constitute aviation obstacles. According to the latest data on the causes of air accidents, aviation obstacles belong to the group of the highest risk factors that contribute to such accidents [3], [4].

Currently, aerial photogrammetry may be the most efficient technique of collecting data about obstacles. It is less automated than such other techniques as the airborne laser scanning (ALS), traditional ground measurements or synthetic aperture radar (SAR), in particular for elongate objects [5]. Low-cost UAVs that ensure high time resolution provide digital images that are then used to create dense clouds of points describing 3-D objects. However, the need emerges to develop process automation in order to overcome the challenge of detecting air obstacles in form of elongate objects. The detection of such objects is difficult and, in fact, they may be detected only from lower altitudes, which are offered by UAV [5].

Point cloud segmentation is the primary step in 3-D point cloud processing. Considering a set of point clouds, the segmentation process aims to aggregate points with similar characteristics into homogeneous regions. The segmentation process can be helpful in scene analysis in various aspects, such as locating and recognizing objects, classifying, and extracting features of these objects [6], [7]. In general, the analyzed objects and their elements have unique geometrical features. Therefore, 3-D geometric features are used as basic information in object detection and categorization of its subelements [8]. 3-D point clouds are optimal for determining the geometric properties of objects. So far, oblique aerial images have been a suitable source for generating 3-D point clouds for object analysis because they provided detailed information about individual object elements: roofs, elevations, etc. Currently, UAVs offer photos with very

high coverage and high resolution, generating very dense 3-D point clouds in a minimum time and with a minimal financial outlay [9]. Thus, low-level 3-D point clouds have become more and more widely used to study 3-D objects.

The point clouds used so far from ALS are accurate and give ready 3-D data. However, the main disadvantage of ALS point clouds is that they are expensive to obtain [10]. For buildings, ALS can only capture the roof and other parts of the building that are only visible from a bird's eye view, and those visible from ground level, such as areas under balconies and building walls that are obscured, are not acquired. Maltezos and Ioannidis [11] argue that the LIDAR point clouds give false results because they misinterpret buildings with smooth roofs.

ALS involves high costs of using specialist photogrammetric equipment during the flight. As the UAVs are equipped with RTK receivers (positioning with the accuracy of one decimeter), the time of data collection and acquisition is very short, e.g., 25 hours are required to obtain and process 1000 ha. The overall costs of collecting and obtaining data with use of UAV may be even several times lower than with use of ALS [68]–[70]. Apart from that, the point clouds obtained from ALS are characterized by lower accuracy than the dense cloud of points generated as a result of processing the image structure from motion (Pix4D, Metashape-type software) from UAV. Images from UAV that are used in the developed method of detecting aviation obstacles are a source of 3-D data that reach the quality standards similar or even higher than those provided by ALS.

Object detection in a 3-D point cloud, segmentation of points belonging to an object, reconstruction of geometry, and object topology are the essential components in the process of 3-D object modelling.

The following section presents a literature review on the classification and segmentation of 3-D objects using photos obtained from UAVs. Additionally, the latest related works on classification and segmentation are presented.

A. Aviation Obstacles

High artificial or natural vertical objects (obstacles) situated near the runway can contribute to accidents during the take-off and landing. The automation of the object detection process in the vicinity of the airport is thus becoming extremely important and necessary for ensuring security around the airport areas. Safe movement at airports and on arrival areas in take-off areas, landing and maneuvering, is an essential element of air traffic safety. Terrain and obstacle data are key geospatial components of aeronautical information. There are international ICAO regulatory documents [2] and national aviation regulations that specify the requirements for collecting and assessing terrain and obstacle data. According to the ICAO, boundary surfaces correspond to the maximum allowable heights of objects in the traffic areas of aircraft. Few studies are dealing with the problem of detecting aviation obstacles in the vicinity of airports. Mitsevich [12] presented remote and effective obstacle identification and assessment process technology using stereoscopic remote sensing. Demir and Baltsavias [13] focused on the accuracy, resolution, and timeliness of data about objects in the vicinity of airports and the automation of 3-D model generation processes using airborne laser scanning. In another work by Demir *et al.* [14], the authors focused on detecting buildings in the airport environment by combining information from aerial imagery and LIDAR data. They used four different methods. The first was based on a DSM/DTM comparison combined with an NDVI analysis. The second was the supervised multispectral classification refined by the standardized DSM. The third approach used empty spaces in the Lidar DTM and NDVI classification (method 3), while the last method was based on the density analysis of Lidar DTM and DSM raw data. A study by Parrish and Nowak [15] presents the methodology of modelling objects using very dense, detailed point clouds, in which the vertical structures of objects are well characterized. The existing recommendations [5] concerning the detection of aviation obstacles focused on using point clouds from ALS. However, as one cannot exclude omitting elongate obstacles, object detection is verified with use of traditional ground measurements, which significantly increased the duration of the process. Additionally, ALS does not ensure high time resolution of data. In terms of ensuring safety in the air space, time resolution and accuracy of data on aviation obstacles are of key importance in performing aviation operations. Objects that are taller than the boundary surfaces, in certain conditions may cause the need to increase the relative or absolute altitude of flight above the obstacles for precision instruments landing approach or any other flight procedure. Such objects may also have an operational influence on designing flight procedures. There is no doubt that the accuracy of determining aviation obstacles affects the safety during the flight of an aircraft [12].

According to the latest provisions of the Eurocontrol manual [5] the detection of elongate aviation obstacles should be ensured at a much higher image scale than that obtained from traditional photogrammetric missions.

B. Segmentation

Segmentation [16] is one of the critical phases of point cloud processing. It aims to group the points into significant clusters with homogeneous properties [17]. Point cloud segmentation, the aggregation of 3-D points into many homogeneous groups with standard features [18], has been studied for decades. A majority of the authors have focused on designing and developing hand-made algorithms for point classification and [19]–[29]. However, finding the optimal segmentation method remains a challenge [30].

Conventional segmentation methods such as region growing [31] or clustering examine points in the vicinity of initial seeds or origins and check if they belong to the same group or not according to the given criteria. Euclidean distance [32], density [33], [34], vector normal deviation [35], [36], surface smoothness [37], and curvature [38] of points are representative criteria. Besides, segmentation may also be performed in the feature space. Distinctive geometric features or RGB information are also

introduced as segmentation criteria [39]. However, all these segmentation methods are easily affected by noise and outliers in the dataset, resulting in over- or undersegmentation with different granularities of the segments obtained. Besides, complex segmentation criteria will significantly increase the computational time. In addition, the gaps between the point clouds (mismatch of the points from the image matching for each pixel of the image) and different point densities make this a more problematic issue. Overall, point cloud segmentation can be considered a difficult topic.

The review of methods, algorithms and solutions that can be applied at individual modelling stages is provided in [40]. At the last stage of modelling, buildings are usually formed as a combination of planes in 3-D space. For this reason, the second stage of the modeling process is crucial, as this is when subsets of points describing (modeling) individual planes are extracted. This task is complicated by the presence of erroneous points in the set. At this stage, the most commonly used algorithms are RANSAC, rising planes, and the Hough transform, with possible modifications, with the first two of the methods mentioned above being dominant.

In their research, Nguyen and Le [41] presented segmentation methods divided into five categories: edge-based; region-based; attribute-based; chart-based; and model-based. In model-based methods, all points with the same mathematical characteristics are grouped into a single segment, such as a sphere, plane, and cylinder. Schnabel *et al.* [42] proposed a model-based algorithm for detecting basic shapes from disordered point clouds. Their algorithm is based on RANSAC. In their works, Bauer *et al.* [43] and Boulaassal [44] use the RANSAC algorithm to detect building facades. To optimize the operation of this estimator in the plane extraction process, it has undergone numerous modifications. Awwad *et al.* [45] and Delmerico *et al.* [46] propose to consider the direction of the normal vector calculated at each point of the cloud. Concerning the detection and modeling of aviation obstacles, the application of several algorithms was presented, which allow to isolate the shape of obstacles and to adjust the point cloud [52], [53]. Knowing the height and location of the obstacles is sufficient for the aircraft to avoid them. Several other methods of detecting aviation obstacles have also been presented in subject literature [54], [55].

The authors of this article will attempt to prove the following hypothesis: point cloud segmentation with the modified RANSAC algorithm through the use of vector data parameter, the introduction of a new point cloud classification algorithm, which is adapted to the geometric features of aviation obstacles, and the criterion of point cloud filtration obtained from low altitude will allow for the detection of aviation obstacles with an accuracy compliant with ICAO regulations [56]–[59].

The research aimed to develop a methodology for automatic detection of aviation obstacles being elongated objects and their classification based on dense matching of UAV images.

The rest of this article is organized as follows: in Section II, the test data are introduced. In Section III, the research method is explained. Section IV presents experimental results. In Section V, the results are discussed. Finally, Section VI concludes this article.

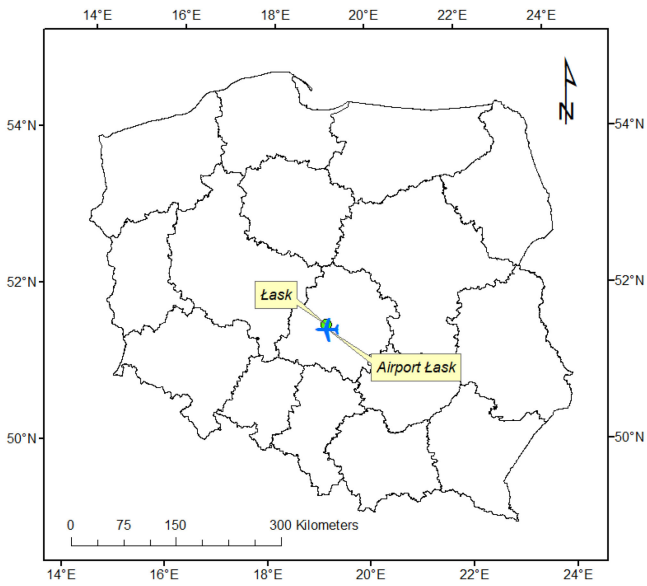

Fig. 1. Location of the Łask military airport.

(a) (b)

Fig. 2. (a) Trimble UX-5 – before flight. (b) Example of GCP location.

II. Materials

A. Study Area

The research was carried out on several selected experimental areas, which were located around the Łask military airport. It is an Air Force airport located in central Poland, south of the town of Łask (51°33′06″N; 19°10′45″E) (see Fig. 1). The surface of the area covered with photos was approx. 25 km^2.

B. Description of the Dataset

The source data for the dense point cloud generation was obtained using the Trimble UX-5 airframe [see Fig. 2(a)], equipped with a Sony a7R camera. The aerial platform was equipped with a single-frequency GPS receiver, recording data at a frequency of 10 Hz.

The flights were carried out in the test area in April 2019. The weather conditions were good, i.e., the sky was covered with a small number of cumulus clouds, and the average wind speed was about 2 m/s. Camera settings were defined in manual mode, while the focus of the lens was set to infinity. The test area covered the area around the Łask military airport. The measurement campaign consisted of 30 test blocks, where each block

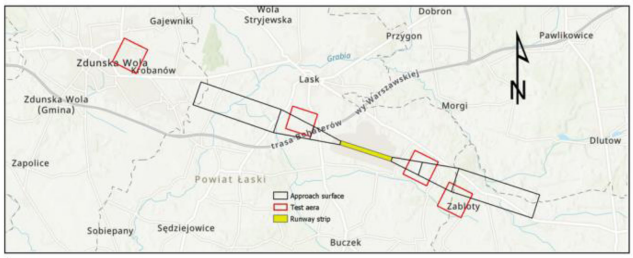

Fig. 3. Research areas.

TABLE I
CHARACTERISTICS OF THE TEST EXPERIMENTAL AREAS IN ŁASK

Experimental area number	1	2	3	4
Number of lines	18	17	16	17
Number of photos	608	576	565	580
Camera / lens focal length [mm]	Sony a7R /36.34			
Average longitudinal/transverse coverage [%]	75/75			
Flight altitude [m]	300			
Number of control points	4	6	5	6
Number of independent checkpoints	5	8	5	7
Value of the standard deviation of a'priori control points and checkpoints X, Y, Z [m]	0.03, 0.03, 0.03			
GSD [m]	0.04			

consisted of approximately 600 images on average. The data was obtained from about 250 m altitude above the ground. The flights were carried out in the east-west direction, assuming that the transverse and longitudinal coverage was 75%. In the study area, the marked control points were designed and measured [see Fig. 2(b)]. All points were measured using the RTK technique in the GNSS system. The terrain coordinates of the control points were determined with the mean error $m_{x,y,z} = \pm 0.03$ m.

C. Characteristics of the Experimental Area

Four experimental areas (1, 2, 3, and 4) were used for further research (see Fig. 3).

They were located close to the runway strip of the Łask airport. The 1st area consisted of 18 lines, 608 photos; the 2nd area included 17 ranks consisting of 576 photos. The 3rd area consisted of 16 lines with 565 photos, and, finally, the 4th area consisted of 17 lines with 580 photos (see Table I).

For the experimental areas, ground control points (which are used in the aerotriangulation process to determine elements of external orientation of images) were measured, as well as independent checkpoints to assess the accuracy of alignment of the block. All images are oriented to the Polish national coordinate system PL-2000 zone VI.

The military airport with the 32nd Tactical Air Base (BLT) is located in Łask (see Fig. 4). The recent modernization of the

Fig. 4. Diagram of the Łask airport based on [aip mil].

airport, i.e., extension of the runway and the modernization of the airport infrastructure, has made the 32nd BLT one of the most modern units of the Polish Air For, pce.

D. Experimental Areas

The research used data obtained from four flights (see Fig. 3). Each of the flights was carried out in the vicinity of the Łask military airport. The first criterion for selecting the research area was to fit into the area coinciding with one of the obstacle limiting surfaces, i.e., the approach surface. The second criterion was the presence of objects protruding above the ground surface, which may pose a potential threat to aircraft traffic. Due to the negligible number of obstacles in the vicinity of the Łask military airport, the research ignored the top-down dimensions and slopes of the approach surface in Poland [60]. That change allowed for the extension of the scope of the study, so that studies could be performed for a larger number of data. Additionally, the developed methodology was universal and possible to use under various constraints and limitations.

1) First Experimental Area: The first area was located very close to the runway of the Łask military airport. Four control points and five independent checkpoints were identified in the study area. Small, heterogeneous buildings characterized the studied area.

2) Second Test Area: The second area was approximately 20 km from the runway. In the study area, six control points and eight independent checkpoints were measured. Most of the area was covered with high, compact buildings.

3) Third Experimental Area: The third area was located approximately 3 km from the runway strip. In the three study area, five control points and five independent checkpoints were determined. The research area was distinguished by small buildings and the presence of numerous power lines.

4) Fourth Experimental area: The fourth area was approximately 10 km from the runway strip. Six control points and seven independent checkpoints were identified in the study area. The site is characterized by scattered development.

E. Obstruction Identification Surfaces

The airspace around the airport should be clear of all aviation obstacles to enable the safe conduct of flight operations and to prevent the airport from being unusable due to obstacles forming in its vicinity. This objective is achieved by establishing

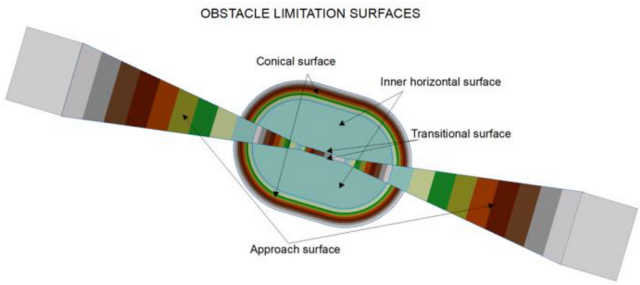

Fig. 5. Obstacle limitation surfaces based on [56].

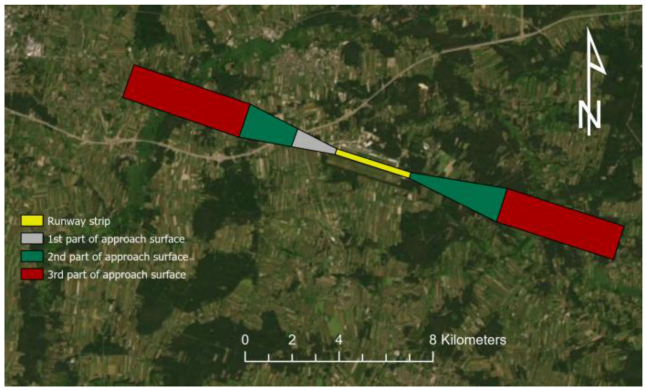

Fig. 6. Obstruction identification surfaces for the Łask military airport based on [56].

a series of obstacle limitation surfaces that define the limits to which objects in the air can protrude. Objects that exceed the obstacle limitation surfaces under certain conditions may require an increase in the altitude or obstacle crossing altitude for instrument approach procedures or any other circular visual flight procedure. These objects may also have an operational impact on the design of flight procedures.

Obstacle limitation surfaces at aerodromes for airplanes shall be established considering the number and location of runways at the airfield, airfield reference code digits, landing approach category, and visual aids for navigation. The dimensions and slopes of the obstacle limiting surfaces for the runways for the Łask military airport have been determined based on Annex 3 to the Aviation Obstacle Ordinance [60], obstacle limiting surfaces and devices of a hazardous nature. Obstacle limiting surfaces include but are not limited to a conical surface, an inner horizontal surface, a transitional surface, and an approach surface (see Fig. 5).

An approach surface is an inclined plane or pattern of planes located at a specified distance from the runway strip. The approach area for the Łask military airport consists of three planes (see Fig. 6). The first (1) plane is 3000 m long and rises by 2%, the second (2) plane is 3600 m long and rises by 2.5%, and the third (3) plane is 8400 m long and horizontal. The approach surface boundary determines the height which objects in the airspace in the vicinity of the airport can reach.

TABLE II
TYPE OF AVIATION OBSTACLE

Type of aviation obstacle	
Mast, antenna	
Wind turbine	
Building, skyscraper	
Chimney	
Tower	
Energy pole	

F. Characteristic of Aviation Obstacles

Aviation obstacles are all fixed (permanent or temporary) or movable objects or their elements that:

1) are located in the zone designated for the movement of air vessels on the ground; or
2) exceed a specific surface designated to protect the air vessel during the flight; or
3) remain outside those defined surfaces, but have been classified as threats for air traffic [5], [57].

Data about aviation obstacles are necessary for the design of landing approach procedures, the creation of aeronautical charts and base databases, and the analysis of aircraft operating limitations. The collected data may also determine the height restrictions or the removal of obstructions that pose a risk to air navigation [57]. The following types of elongated aviation obstacles are listed in the register of aviation obstacles or marked on aerial charts: masts and antennas; wind farms (i.e., wind turbines); buildings, blocks and skyscrapers; chimneys; towers; energy poles (see Table II) [5]. The aviation obstacles listed above represent man-made objects.

III. METHODS

This section introduces and describes a mathematical model that can be used to automatically detect aviation obstacles and classify them based on a random point cloud obtained from a low altitude. The entire process is shown using a flowchart (see Fig. 7). The diagram shows the stages of detection of objects in the vicinity of the airport, assuming that objects above a certain height are considered obstacles to the air. The first stage consisted in acquiring photos from a low level. Then, using the Pix4D software, the images were processed, and point clouds were generated for the various research areas. The works started with the automatic filtration of the point cloud, where the height of aviation obstacles above the approach surface was adopted as the filtration criterion. Then, point cloud segmentation was performed to determine obstacles to aviation. This process started with the implementation of vector data about 2-D objects on the basis of an orthophotomap. The attributes of 2-D objects were directly loaded into segmented point clouds. The use of

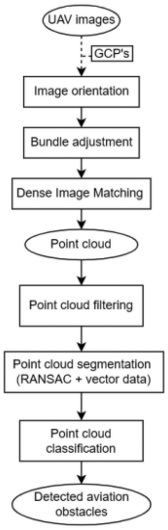

Fig. 7. Scheme of detection of the aviation obstacles.

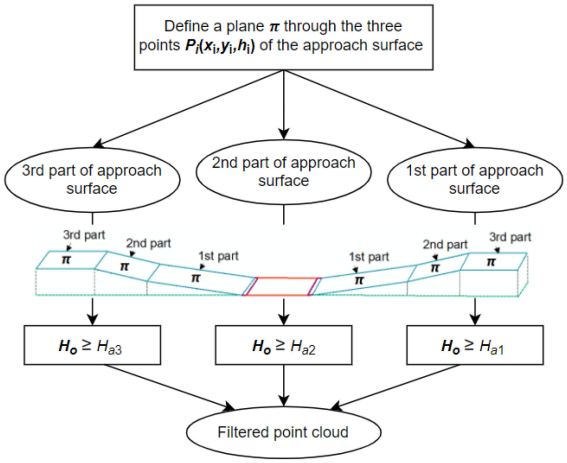

Fig. 8. Scheme of filtering of point clouds.

the geometry of the examined objects made it possible to fit the point cloud into the obstacle database precisely and save the attributes from the 2-D layer to the structure of each segmented point cloud. The final stage was the automatic classification of the point cloud based on the ratio of the object height to its width and geometric relationships of the cross-section of the objects. This classification made it possible to determine the type of obstacle, where GCP's is ground control points.

A. Aviation Obstacle Detection

This section describes the raw point cloud filtering to identify points that may be part of aviation obstacles. The point cloud filtration was carried out in the vicinity of the airport for the area contained in the obstacle limiting surface, called the approach surface. The primary purpose of point filtration was to detect points on or above the approach surface automatically. At this stage, filtered point cloud applied only to the filtration of point clouds by their height, according to the set criterion H_0 (see Fig. 8). The use of the altitude criterion made it possible to detect points that may belong to aviation obstacles (see Fig. 8),

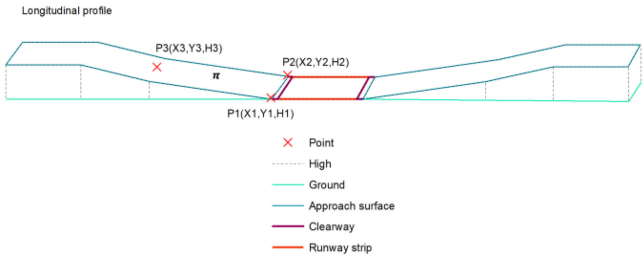

Fig. 9. Approach surface—longitudinal profile.

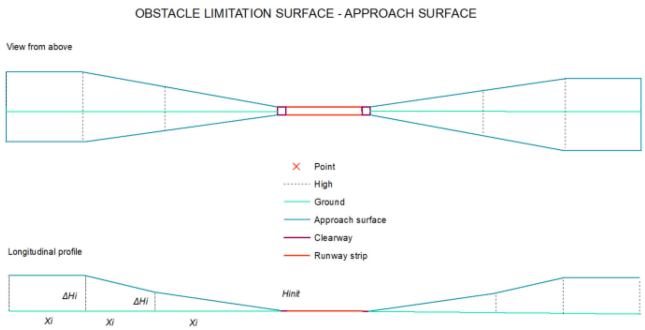

Fig. 10. Obstacle limitation surface—approach surface (plan view and cross section).

where π is planes of approach surface, *Pi(xi, yi, hi)* is points belonging to the π plane, H_o is the height of the obstacle, H_{a1} is the height of the approach surface for the first plane, H_{a2} is the height of the approach surface for the second plane, and H_{a3} is the height of the approach surface for the third plane.

The first stage of point plane cloud filtration involved defining a plane that would uniquely identify points belonging to the approach surface. For this purpose, the equation π (1) passing through three points was used. Every three noncollinear points $P_i(x_i, y_i, h_i)$, where $i = 1, 2, 3$, define exactly one plane π that contains it. The equation for this plane has the form

$$\pi: \begin{vmatrix} x - x_1 & y - y_1 & h - h_1 \\ x - x_2 & y - y_2 & h - h_2 \\ x - x_3 & y - y_3 & h - h_3 \end{vmatrix} = 0. \quad (1)$$

This is called the determinant equation of the plane. The extreme points being the beginning of the approach surface were adopted as point $P_1(x_1, y_1, h_1)$ and point $P_2(x_2, y_2, h_2)$, (see Fig. 9). Point $P_3(x_3, y_3, h_3)$ is at the end of the approach surface passing through the axis of the runway at a distance *n* from the edge of the runway strip.

After defining the planes π of the approach surface, the point cloud was filtered with the height of the H_i points as the main filtering criterion. The airspace object on the approach surface has a specified H_o height. If the H_o is equal to or greater than the height of the approach surface, then the object is considered an obstacle to flight (see Fig. 10).

For the first part of the approach surface, the object will be an obstacle if

$$H_o \geq H_{a1}. \quad (2)$$

The approach surface height was calculated using the following formula:

$$H_{a1} = X_i\, i + H_{\text{init}}. \tag{3}$$

where X_i is the distance from the runway and H_{init} is the height above sea level at the end of the runway.

For the second part of the approach surface, the object will be an obstacle if

$$H_o \geq H_{a2}. \tag{4}$$

The approach surface height was calculated using the following formula

$$H_{a2} = X_i\, i + H_{a1} \tag{5}$$

where X_i is the distance from the runway.

For the third approach plane, an object will be an obstacle if

$$H_o \geq H_{a3}. \tag{6}$$

The 3rd approach plane height, a horizontal surface, is equal to the maximum height of second plane and is constant

$$H_{a3} = \text{constans}. \tag{7}$$

The points above the designated planes were classified as obstacle points and used for further research. Points below the plane did not constitute aviation obstacles; therefore, they were omitted in further studies.

B. Point Cloud Segmentation

The second part of the methodology is the extraction of flat features using the RANSAC algorithm operating on nonground points classified in the previous step.

A new vector data parameter has been added to the RANSAC algorithm, defining the shape and attributes of the tested objects (aviation obstacles).

The RANSAC algorithm is an iterative method used to estimate the parameters of the searched mathematical model of an object in a data set containing a significant number of points not belonging to the modeled surface [61], [62]. That fact makes the RANSAC estimator particularly interesting for processing point clouds with noise and erroneous measurements. The algorithm's operation consists of two phases: initialization and test, repeated iteratively (see Fig. 11). The initialization phase was preceded by creating 2-D vector data on the basis of an orthophotomap for the detected aviation obstacles, containing information about these obstacles and automatic loading of vector data in the .shp format, where i is initiation stage, CS is consensus set, t is number of points matching the set, M_t is model, S is data, P is plane, M_d is maximum distance between the tested point and the hypothetical model, p is point matching the model, d is distance between the point and the assumed model, s_t is minimum sets, T_{iter} is number of minimum sets, k is the smallest number of data necessary to unambiguously define the assumed geometric model, ε is probability of identification of the wrong plane, and t_{rest} is threshold value.

The initialization stage consisted in randomly selecting the minimum set of points that are necessary for the unequivocal determination of the parameters of the estimated geometric model.

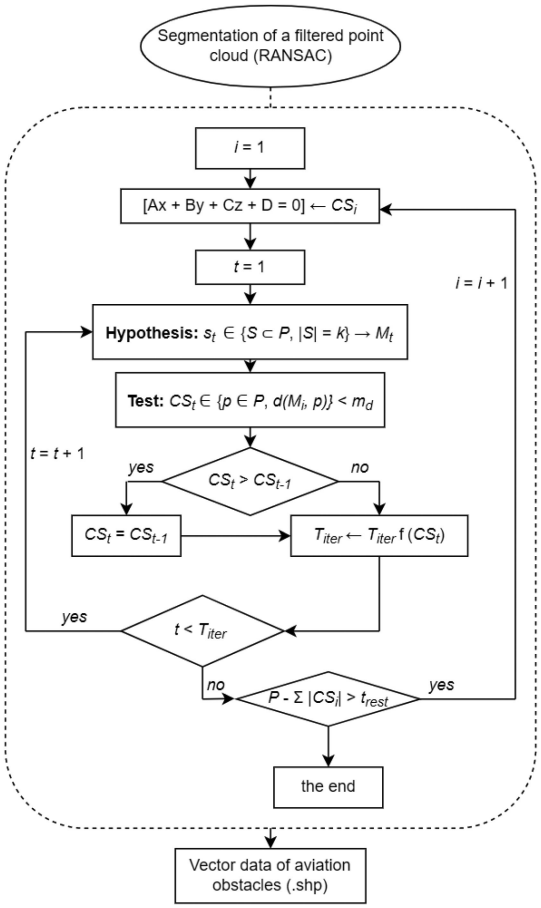

Fig. 11. Point cloud segmentation—algorithm RANSAC and vector data of aviation obstacles.

It is the smallest number of k data necessary to unequivocally define the assumed geometric model. For plane extraction, the minimum set consists of three points. The implementation of the algorithm begins with the drawing of a predetermined number of T_{iter} of minimal sets s_t (8), which is successively modified during the algorithm

$$s_t \in \{S \subset P,\, |S| = k\} \rightarrow 1 \tag{8}$$

Next, the parameters of the Mt model are calculated for each of the sets (in the case under consideration, the model is a plane passing through three points). The identified model is a hypothesis that is tested in the next step—the test. The test stage requires the determination of the value of the m_d parameter, which defines the maximum distance of the tested point from the hypothetical model. If the point meets the distance criterion, it is added to the so-called *CS* (Consensus Set). In this article, the set consists of data that were considered to belong to the considered plane: Σ

$$CS_t \in \{p \in P,\, d(M_i,\, p)\} < m_d \tag{9}$$

where

$$d(M_i,\, p) \tag{10}$$

determines the distance of the point from the assumed model [63].

After performing the test (9) for all data, the next minimal set is selected as the basis for the sequence of two steps—hypothesis and test—that are then repeated. If a CS set containing a greater number of points than the previous one is found, the existing set is replaced with the more numerous one and the T_{iter} value is modified (number of samples of the minimum sets)

$$T_{\mathrm{iter}} = \frac{\log \varepsilon}{\log (1-q)}. \tag{11}$$

where ε is the probability of identifying the wrong plane, and q is calculated from the following equation [64]

$$q = \left(\frac{N_I}{N}\right)^k. \tag{12}$$

wherein

N_I is number of points belonging to the identified plane,
N is number of all points belonging to the input data set, and
k is the smallest number of data allowing for an unambiguous determination of the model.

When the identification of the first plane is completed, the described process is repeated, except for the points qualified to it. Identification of successive planes is completed when the number of points not added to them is lower than the assumed threshold value of t_{rest}.

C. Point Cloud Classification

The point cloud classification was aimed to detect aviation obstacles representing a specific group of elongated objects with regular cross-sections. The first criterion was the height of the objects determined based on point clouds. The second classification criterion was based on the geometric properties of objects formed by point clouds (see Fig. 12), where w_o is the obstacle width and H_o is the obstacle height.

It was assumed that for objects belonging to the group of obstacles: masts, wind turbines, chimneys, towers, power poles and skyscrapers, the ratio of the width w_o of the object to its height H_o [65] should be within the following range:

$$\frac{1}{10} < \frac{w_o}{H_o} < \frac{1}{2}. \tag{13}$$

For aviation obstacles belonging to a group of buildings, the ratio of the width of the object w_o to its height H_o should be in the range:

$$\frac{w_o}{H_o} \geq \frac{1}{2}. \tag{14}$$

The height of aviation obstacles was determined in iterations, based on the cloud of points. Points that belonged to a plane at a certain height were searched in the dataset. Point searches were performed at 10-cm intervals, until the top point of the obstacle was found. This point was the basis for determination of height. The divisions for classifying obstacles, considering their width and height, were determined at the confidence level of $\Pr(\mu - 1\sigma \leq \mathrm{X} \leq \mu + 1\sigma) \approx 68.27\%$. Obstacles that did not fall into the ranges described above (13, 14) did not meet the adopted criteria for elongated objects, so they were excluded from further stages of the analysis.

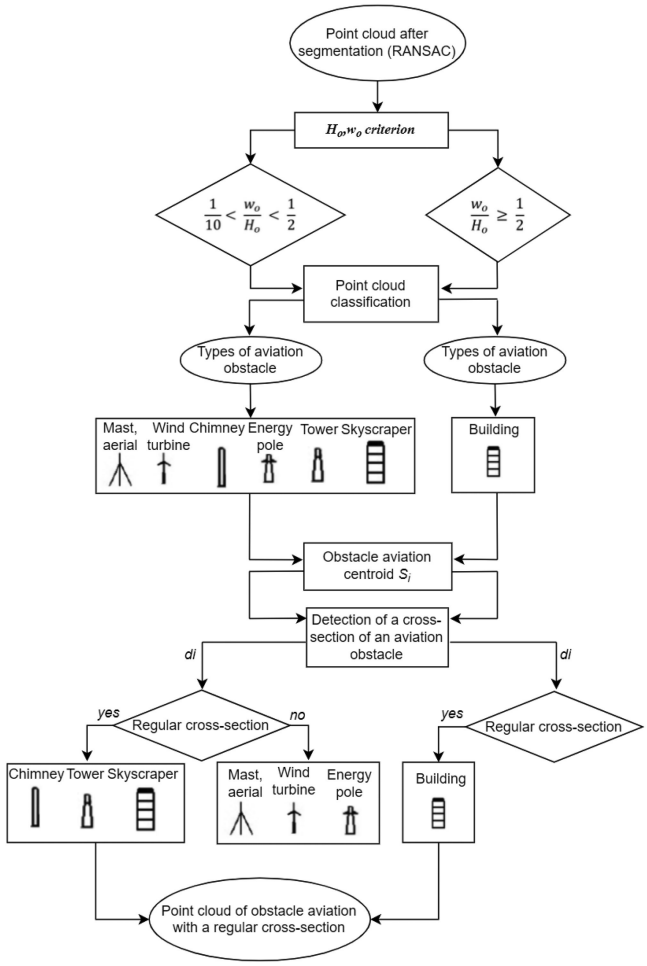

Fig. 12. Aviation obstacle filtration process.

The point clouds assigned to the appropriate groups of obstacles were classified according to their cross-sections. For this purpose, for each object, its centroid Si was determined by calculating its coordinates (x_s,y_s) based on the following formulas:

$$x_S = \frac{\sum x_i}{n} \tag{15}$$

$$y_S = \frac{\sum y_i}{n} \tag{16}$$

where x_s is x coordinate of the centroid [m], y_s is y coordinate of the centroid [m], and n is number of points in the point cloud of the tested object.

The tested objects were classified based on the distance d_i [see Fig. 13(a) and (b)] of each point cloud point from the object's centroid *Ci*. The distance of the points from the centroid was calculated using the following formula:

$$d_i = \sqrt{(x_S - x_i)^2 + (y_S - y_i)^2} \tag{17}$$

where d_i is the distance of the points from the centroid, x_s is x coordinate of centroid [m], y_s is y coordinate of centroid [m], x_i

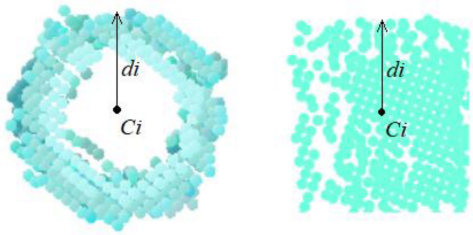

Fig. 13. Cross-section of an aerial obstacle. (a) Circular. (b) Polygonal.

is x coordinate of a point from a point cloud [m], y_i is y coordinate of a point from a point cloud [m].

Based on the distance of the point cloud along object edges, a group of regular and irregular cross-section objects was defined. For objects with a typical cross-section, it was assumed that if the distance from the extreme points of the cloud of points constituting the object's edge is constant, we are dealing with objects with a circular cross-section [see Fig. 13(a)]. On the other hand, if the distance from the extreme points of the cloud of points constituting the object's edge was not constant, we are dealing with objects whose cross-section was a polygon [see Fig. 13(b)]. Therefore, objects such as chimneys, towers, buildings, and skyscrapers were classified as objects with a regular cross-section. Objects with an irregular shape included masts, wind turbines and power poles. Objects classified as regular (i.e., typical cross-section) were used for further research.

IV. Experiments and Results

This section presents the research experiments and the corresponding results obtained from the UAV images. Initial filtration of the point cloud was performed to detect objects that exceed the boundary surfaces, i.e., aviation obstacles. Then, using the RANSAC algorithm, segmentation of the point cloud was performed. The final stage consisted in the automatic segmentation of the point cloud based on the geometric relationships in the detected objects, which allowed for the selection of objects of a regular cross-section and uniform shape. During the experiment, the authors attempted to use the developed method to detect obstacles of irregular cross-sections and shapes, such as poles, masts, and antennas, but the obtained results were difficult to interpret.

A. Generating a Dense Point Cloud

After determining the external orientation of the photos, the so-called "rare" 3-D point cloud, which is the starting position to generate the so-called "dense" point cloud, the point cloud was generated using the image matching algorithm. The point cloud extraction process requires relatively small effort, as the only input elements are photos with external orientation. The results of the point cloud compaction are presented in Table III. The RMS error of the 3-D point location for the first test area was 0.02 m, for the second test area 0.01 m, for the third test area 0.03 m, and for the fourth test area 0.01 m.

TABLE III
Point Cloud Densification Results

Number of test area	RMSE 3D point [m]	Average Density (per m3)
1	0.02	81.62
2	0.01	80.22
3	0.03	77.20
4	0.01	80.49

Fig. 14. Łask military airport—location of the terrains profiles.

B. Assessment of the Height Accuracy of Dense Point Clouds Based on the Terrain Profile

The accuracy of dense point clouds was then assessed by means of the following.

1) Comparing the altitude accuracy of point cloud profiles with the terrain profile measured in the open area using the GPS RTK method,
2) *Semi Global Matching* (SGM): Generated point cloud profiles comparison with LiDAR point clouds [66].

Five field profiles were measured in the study area (see Fig. 14).

Field profiles 1, 2, and 5 were measured in open areas, where the satellite signal reaching the receiver is characterized by the maximum possible strength, which affects the quality of the obtained results. Profiles 3 and 4 ran close to the forest, where growing trees could somewhat disrupt the signal.

The terrain profiles used to determine the precision characteristics of the point cloud were measured for each of the four test areas. Profile no. 1, approximately 750 m long, consisted of 131 points and was measured with an interval of 4–9 m. Profile no. 2, approximately 600 m long, consisted of 91 points, and was measured with an interval of 4–8 m. Profile no. 3 with a length of about 500 m and the number of points 82 was measured with an interval of 5–9 m. Profile no. 4, about 650 m long, consisted of 119 points, was measured from interval 4–9 m. Finally, profile no. 5, about 670 m long, consisted of 123 points.

Based on the differences in height between the examined point clouds and the measured field profile, parameters characterizing the accuracy were calculated, such as the average height difference, maximum negative, and positive deviations, mean error and standard deviation. The results are summarized in Table IV.

TABLE IV
STATISTICAL VALUES CHARACTERIZING THE HEIGHT ACCURACY ALONG THE TERRAIN PROFILE, CALCULATED FOR THE DENSE POINT CLOUDS STUDY

Profile	GSD [m]	Mean height difference [m]	Maximum negative deviation [m]	Maximum positive deviation [m]	Mean error [m]	Standard deviation [m]
1	0.04	-0.06	-0.16	+0.05	0.06	0.07
2	0.04	-0.03	-0.05	+0.10	0.08	0.11
3	0.04	-0.04	-0.04	+0.11	0.08	0.08
4	0.04	+0.03	-0.12	+0.18	0.06	0.15
5	0.04	-0.05	-0.07	+0.09	0.07	0.12

TABLE V
STATISTICAL VALUES CHARACTERIZING THE HEIGHT ACCURACY ALONG THE TERRAIN PROFILE, CALCULATED FOR THE LIDAR POINT CLOUDS

Profile	Density [pt/m^2]	Mean height difference [m]	Maximum negative deviation	Maximum positive deviation [m]	Mean error [m]	Standard deviation [m]
1	4.0	0.09	-0.07	+0.18	0.11	0.06
2	4.0	0.08	-0.06	+0.15	0.09	0.04
3	4.0	0.09	-0.06	+0.18	0.09	0.08
4	4.0	0.10	-0.04	+0.17	0.09	0.07
5	4.0	0.07	-0.08	+0.14	0.12	0.06

Terrain profiles were measured on point clouds obtained from airborne laser scanning. It was assumed that the satellite measurement data are error-free, and that the error would be determined in relation to them.

The assessment of the accuracy of dense point clouds was compared with the parameters characterizing the accuracy of the LiDAR point clouds. The results are summarized in the table.

The data presented in Tables IV and V constitute the basis for assessing the altitude accuracy of SGM point clouds compared to LiDAR point clouds, taking into account the factors influencing the properties of SGM point clouds. Based on the results of the accuracy analysis, several regularities were noticed are as follows.

1) LiDAR point clouds are burdened with a greater systematic error than SGM point clouds.
2) Images obtained from UAV provide a point cloud with greater horizontal accuracy (lower mean error) than LiDAR point clouds.
3) Standard deviation of the LiDAR point cloud is smaller than almost all SGM point clouds.
4) Value of the standard deviation is slightly higher for the SGM point cloud, which indicates that the images obtained from the UAV also provide a point cloud that correctly reflects the topography.

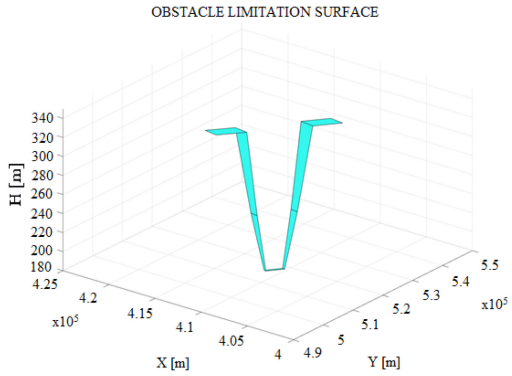

Fig. 15. Obstacle limitation surface as specified in ICAO.

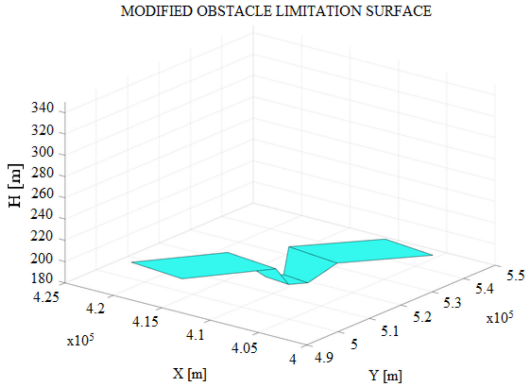

Fig. 16. Obstacle limitation surface as modified obstacle limitation surface.

C. Detection of Objects That are Aviation Obstacles

Dense point cloud became the basis for further research on the detection of aviation obstacles. After the initial processing of data obtained from the UAV and testing the accuracy of the point cloud, the point cloud was filtered. To do so, obstacle limiting surfaces were determined as the initial step in detecting aviation obstacles. The Łask military airport belongs to the first class of airports [2], [60] and has strictly defined surfaces limiting obstacles. Each of these surfaces is at a certain height, and objects whose height is higher than the obstacle limiting surfaces are called air obstacles. The equations of planes π constituting the obstacle limiting surfaces were determined in compliance with the ICAO requirements (see Fig. 15).

Each of the planes rises to a particular height H. This height became the point cloud filtration criterion. Points with a height equal to or greater than the height of the approach surface were classified as elements of aviation obstacles $H_o \geq H_{a1}$ (see Fig. 15) and were used in further stages of the research. During the study, they were introduced to the regulations that define the range of obstacle limiting surfaces. The altitude requirements in the close vicinity of the airport have changed. In the area of the Łask airport, the obstacle limiting surface was modified for research purposes (see Fig. 16) by increasing the range of the surface and lowering the height, which allowed the authors to obtain more research material in the form of further obstacles.

The modified obstacle limitation surface has defined the limit heights above which objects become aviation obstacles. Points

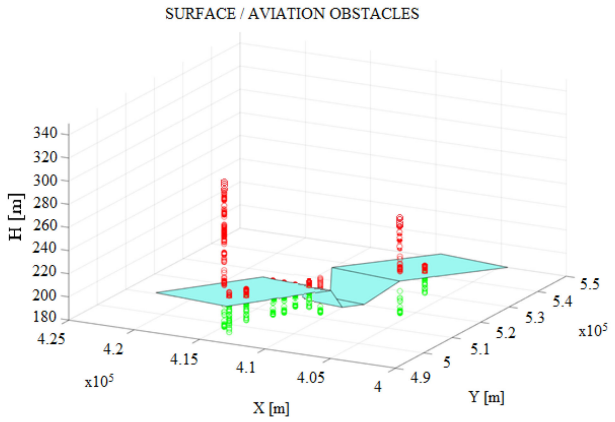

Fig. 17. Modified obstacle limitation surface with aviation obstacles.

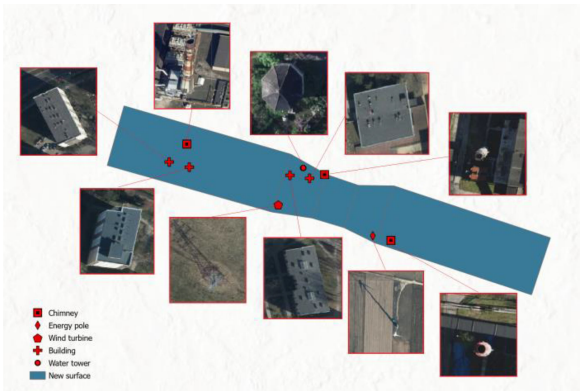

Fig. 18. Location of aviation obstacles near the Łask military airport.

from the point cloud that pierced the limiting surface were used for further development. Ten obstacle objects were detected in the four experimental areas (see Fig. 17). Points below the boundary surface are marked in green. Points above the boundary surface are marked in red.

D. Segmentation and Classification of Point Cloud

After the filtration of the point cloud, ten objects were selected for further analysis as aviation obstacles in the vicinity of the Łask military airport. Three obstacles were chimneys, and four more were buildings; a power line pole; a wind turbine; and the last one was a water tower. All of the abovementioned obstacles were located near the airport (see Fig. 18).

The ten analyzed data sets were characterized by the fact that they represented tall structures. The facilities differ significantly in terms of their architecture. However, three groups of objects may be distinguished based on their cross-section. The industrial chimney is a slender structure but similar in its round cross-section to a water tower. The skyscraper is a tall building, slightly different from the apartment block, but there is an analogy in the cross-section. Both the power line pole and the wind turbine are elongated objects, but their cross-sections are irregular. The primary objective of the research was to develop a methodology for detecting aviation obstacles of an elongated shape, where the main emphasis was placed on the most accurate reflection of their actual height. Given the above, the segmentation algorithm was aimed at the most precise determination of the height of aviation obstacles.

All analyzed objects were segmented and classified to detect their actual shapes and heights. The previously filtered point clouds were used as input data. The implementation of the segmentation algorithm began, on the basis of an orthophotomap, with the creation of 2-D vector data about objects that are aviation obstacles. Then, the vector data in the *X, Y* horizontal planes was implemented in MATLAB. The work began with withdrawing a predetermined number T_{iter} of minimal sets s_t, which were modified online. Then, for the collection of points, the parameters of the plane surface passing through the three points were calculated. The model detected in this way became the hypothesis that was then tested in the next step, i.e., the test. The algorithm started with determining the maximum distance from the tested point to the hypothetical model. If a specific point met the distance criterion, it was added to the so-called set consisting of data that belonged to the considered plane M_t. After the test was performed, the next minimal set was selected. From this set of points, the hypothesis and test steps were repeated. When the algorithm found a set of points with more points than the previous one, the existing set was replaced with the larger set. After the detection of the first plane, the whole process was repeated, but without the participation of points belonging to the first plane. The plane detection was performed until the number of points not added to any of the planes was lower than the assumed threshold value of t_{rest}.

The presented algorithm was applied to all four data sets, which enabled the detection, segmentation and classification of the point cloud. The input data for all examined objects was the point cloud of individual objects. The first photogrammetric treatment was an industrial chimney. In this case, the algorithm detected the object automatically and quickly. As a result of the application of the RANSAC algorithm, data on an obstacle with known coordinates *X, Y, H* were obtained (see Fig. 19). The height of the obstacle was determined with an accuracy of 0.03 m. The second tested object was the water tower. Both the tower and the chimney have a common feature—despite the different architectural styles, both buildings have circular cross-sections. The water tower data set was characterized by the lowest number of points among all the tested objects. In this case, the input data set consisted of 20 thousand points. Here, the segmentation of the point cloud allowed the detection of the water tower, which was an aviation obstacle. The following data sets were much more numerous, and the number of their elements was in the range of 115 000 points up to 150 thousand. The clouds of points corresponding to the power line pole and wind turbine were also subjected to segmentation. In these two cases, the obtained results were ambiguous, so obstacles with an irregular cross-section were excluded from the subsequent part of the research. The last segmented objects were two industrial chimneys located in the vicinity of the airport.

E. Comparison of Segmentation Results

The preliminary analysis of UAV point cloud segmentation results was carried out based on a comparison with the segmentation results for the point cloud obtained from airborne

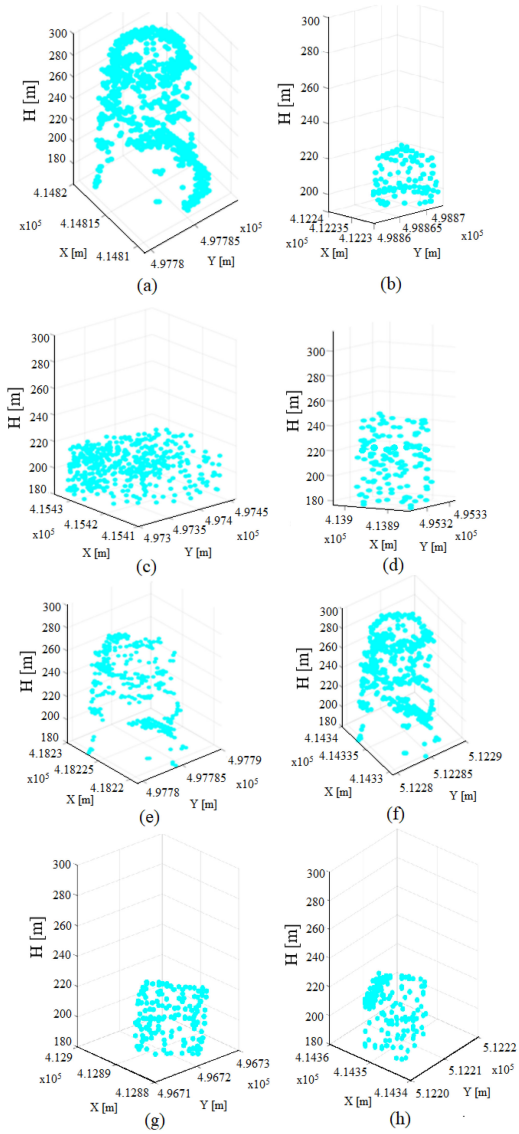

Fig. 19. Detected aviation obstacles. (a) Chimney. (b) Water tower. (c) Building. (d) Building. (e) Chimney. (f) Chimney. (g) Building. (h) Building.

laser scanning. All correctly detected aviation obstacles were analyzed. It was noticed that in the case of both groups of data, the RANSAC algorithm, in most cases, correctly qualified the points belonging to objects that were aviation obstacles. The LiDAR point cloud was characterized by a more significant, evenly distributed number of points on the ground and base. The algorithm incorrectly qualified the ground points to the set belonging to the obstacle. The analysis of segmentation results for both data sets has been extended to include a summary of the algorithm execution time, processing data sets of various sizes (see Table VI). Based on the outline of the results, one may notice that the number of points does not increase the number of surface planes and thus the time needed to perform the segmentation.

F. Analysis of the Accuracy of the Point Cloud Fit

The analysis of the accuracy of the point cloud fit was carried out based on the reference data contained in the eTOD database (electronic Terrain and Obstacle Data). The aerodrome obstacle database includes information on objects penetrating the aerodrome boundary surfaces. The database contains information on the longitude and latitude of the obstacle, its absolute height, height above the ground surface, location—locality, type of obstacle, etc. The analysis of the accuracy of fitting the cloud of points took into account whether it fit into the horizontal plane (*X, Y* coordinates) and fitting into the vertical plane (*H* coordinate) (see Table VII).

The accuracy analysis was carried out for eight aviation obstacles—three industrial chimneys, four buildings, and one water tower located in the vicinity of the airport.

Based on the above table, it can be seen that the average difference in horizontal coordinates (*X, Y*) was in the range from 0.01 to 0.05 m. The average difference in height (*H*) fell in the range from 0.02 to 0.04 m. Mean error of the point cloud fitting to the obstacle data set was from $\pm$ 0.04 to $\pm$ 0.08 m, and the standard deviation ranged from 0.04 to 0.07 m.

TABLE VI
SUMMARY OF THE ALGORITHM EXECUTION TIME FOR THE UAV POINT CLOUD AND LIDAR POINT CLOUD

Obstacle	Number of points UAV	Number of points LiDAR	Number of planes UAV	Number of planes LiDAR	Time UAV [s]	Time LiDAR [s]
1 (chimney)	841	952	5	5	10	11
2 (chimney)	798	818	4	4	9	11
3 (chimney)	803	812	4	4	9	10
4 (building)	1404	1558	3	3	12	14
5 (building)	1656	1688	5	5	18	19
6 (building)	1894	1902	7	7	21	22
7 (building)	1528	1533	6	6	19	21
8 (water tower)	702	731	3	3	9	10

TABLE VII
STATISTICAL VALUES CHARACTERIZING THE ACCURACY OF THE POINT CLOUD FITTING

Obstacle	Mean X coordinate difference [m]	Mean Y coordinate difference [m]	Mean height difference H [m]	Mean error [m]	Standard deviation [m]
Chimney 1	0.02	0.03	0.03	0.05	0.04
Chimney 2	0.03	0.01	0.04	0.07	0.06
Chimney 3	0.02	0.02	0.02	0.04	0.06
Building 1	0.04	0.03	0.03	0.06	0.07
Building 2	0.05	0.04	0.02	0.07	0.07
Building 3	0.03	0.02	0.04	0.06	0.05
Building 4	0.02	0.05	0.04	0.06	0.05
Water tower	0.02	0.03	0.03	0.04	0.05

Based on the accuracy results, it can be concluded that the developed method of aviation obstacle detection and classification guarantees horizontal and vertical accuracy at the level of several centimeters.

V. Discussion of Results

This section covers the results of detection, low altitude point cloud segmentation, and elongated aviation obstacle classification.

The research on the algorithm of aviation obstacle detection was preceded by an analysis of the altitude accuracy of dense point clouds based on the measured terrain profiles. For this purpose, the accuracy parameters were calculated based on the differences in height between the dense point clouds and the measured terrain profiles. The standard deviation ranged from 0.07 to 0.15 m. The accuracy assessment was supplemented with the measurement of field profiles on point clouds obtained from airborne laser scanning. Based on the height determined from ALS point cloud and field profiles, the standard deviation ranged from 0.04 to 0.08 m. The mean error for the dense point clouds was lower by 0.03 m. The standard deviation for the dense point clouds was more significant by 0.04 m than the standard deviation of the LiDAR point cloud. In his research, Wallace *et al.* [67] presented a similar vertical accuracy obtained with the use of ALS and UAV, pointing to the advantage of UAVs due to the relative ease and speed of data acquisition.

The initial detection of objects resulting from automatic filtration of points located above the designated surface allowed for the identification objects that may be aviation obstacles. The processing time of this method and the complete automation of the process demonstrate the high efficiency of the presented approach.

This article presents a modified RANSAC algorithm to perform point cloud segmentation. The algorithm was enriched by adding the parameter of vector data that define the attributes and shapes of the analyzed objects.

The culmination of the aviation obstacle detection process was the automatic classification of the aviation obstacle point cloud based on the width and height of the obstacle as well as on the centroid and the cross-section of the object. Thanks to this method, it was possible to determine to which group the tested point cloud belongs more accurately.

The article focuses on detecting the exact position of an obstacle (X, Y) and its height (H). The obtained accuracy results proved that the RANSAC algorithm is a sufficient method for examining geometrically uncomplicated objects [50]. The authors took an attempt to use the developed method to detect such obstacles as masts, turbines, poles, etc., i.e., objects of irregular shapes. However, the obtained results were ambiguous, so that, at this stage, it remained impossible to detect obstacles other than those of geometrically uncomplicated shapes. In spite of these limitations, the presented method still ensures, among others, the required accuracy for detecting obstacles [56], the automation of the procedure, and shortening the duration of the whole detection process.

The accuracy analysis of aviation obstacles detection and classification has been enriched with creating a synthetic model to determine the accuracy of plane identification. The analysis results made it possible to conclude that the algorithm allows for the determination of the exact location of the planes; however, a slight flaw was noticed, which was the incorrect inclusion of points located in the same plane, but not belonging to the aerial obstacle. However, this did not affect the vertical accuracy of the determined obstacles.

The developed methodology enabled the detection of obstacles of regular cross-sections, with a uniform structure of the point clouds. The positioning accuracy was checked with the obstacle database. The mean error of fitting the point cloud in eTOD was from $\pm$ 0.04 to $\pm$ 0.07 m. The standard deviation ranged from 0.04 to 0.07 m. The mean difference in the X coordinate was from 0.02 to 0.05 m, in the Y coordinate from 0.01 to 0.05 m, and in the H coordinate from 0.02 to 0.04 m. Mitsevich [12] obtained lower accuracy of determining aviation obstacles in this article, achieving accuracy on the level of 0.3 to 0.5 m.

The experiment presented here demonstrates the advantages of using imagery from UAV to detect aviation obstacles. Data from UAV are obtained depending on the needs and the only limitation are the meteorological conditions, while data from airborne laser scanning are obtained usually only once a year. Although the ALS enables to cover a larger area, the necessity to ensure a high frequency of obtaining data, considering the emerging needs, forces us to use a more cost-effective method, which is the UAV.

However, despite the satisfactory results, the presented method has some limitations. The first limitation of the proposed method and other similar algorithms based on statistical image values is that they may not be suitable for specific examples of images, e.g., those obtained in poor weather conditions. An example may be intense fog that obscures only a part of the object captured in the photograph. In that case, the use of the algorithm will negatively affect the color reproduction in the image and, consequently, degrade the spectral quality of the image. Another limitation resulted from narrowing down the research to aviation obstacles that were elongated objects. The developed methodology is used to study objects, which may include towers, chimneys, skyscrapers, or buildings i.e., those that have a regular cross-section and uniform shape. The detection of obstacles of an irregular shape (heterogeneous distribution of the point cloud), such as a power line pole or wind turbine, brought ambiguous results, which suggests that the method still requires further development. The authors are planning to conduct further research to detect all types of aviation obstacles in the vicinity of airports.

VI. Conclusion

The article attempts to describe the automatic detection and classification of elongated aviation obstacles based on dense point clouds. The authors used a modified RANSAC algorithm, presented a new approach to aviation obstacle detection and classification and to point cloud filtration. The main objective of the methodology is to detect elongated aviation obstacles in the close vicinity of the airport.

As a result of the conducted research, eight aviation obstacles were detected, and the obtained accuracy seems to be promising. Based on the data contained in eTOD, the accuracy of

the point cloud fit was calculated. The mean error of fitting the point cloud was ± 0.05 m. The mean difference in the *X* coordinate was from ± 0.03 m, the mean difference in the *Y* coordinate was from ± 0.02 m, the mean difference in the *H* coordinate was from ± 0.03 m—precision limits imposed by ICAO rules [56]–[59]. The authors of this article presented a methodology that enables detecting obstacles of an elongated shape. Tests were conducted on a dense point cloud generated based on imagery obtained from UAV and dense image matching algorithms. So far, research on the detection of aviation obstacles was conducted on point clouds obtained from airborne laser scanning [5]. However, the correct detection of elongated obstacles was difficult and required additional control by means of traditional ground measurements, which significantly increased the duration of the detection process [5]. The method presented here offers higher spatial accuracy, lower data acquisition costs, higher time resolution, i.e., up-to-dateness of data, the possibility to analyze large areas, automation of the process, detecting elongated obstacles, and, finally, shortening the total duration of the detection procedure. The developed methodology may significantly improve the process of analyzing aircraft operational limitations, designing procedures, creating aeronautical charts, and improving safety in the airspace by reducing the risk of an aircraft collision with an obstacle to a minimum. The presented approach can be used for airports of various categories, with differing constraints imposed by obstacle limiting surfaces.

Future research will improve the presented methodology and extend the study to other types of aviation obstacles. The authors plan to expand the classification algorithm to cover all kinds of aviation obstacles.

References

[1] M. Zeybek and İ. Şanlıoğlu, "Point cloud filtering on UAV based point cloud," *Measurement*, vol. 133, pp. 99–111, 2019.

[2] Annex 14 to the convention on international civil aviation, "Aerodromes: Aerodromes design and operations," ICAO, 8th ed., vol. I, 2018. [Online]. Available: https://ffac.ch/wp-content/uploads/2020/10/ICAO-Annex-14-Aerodromes-Vol-I-Aerodromes-Design-and-Operations.pdf

[3] ICAO, "Safety report," Int. Civil Aviation Org., Montreal, Canada, 2020. [Online]. Available: https://www.icao.int/safety/Documents/ICAO_SR_2020_final_web.pdf

[4] ULC, "Sprawozdanie o stanie bezpieczeństwa lotnictwa cywilnego za rok 2019," (in Polish), Urząd lotnictwa cywilnego, 2020. [Online]. Available: https://www.ulc.gov.pl/_download/bezpieczenstow_lotow/analizy/Sprawozdanie_2019.pdf

[5] Terrain and Obstacle Data Manual, Eurocontrol, 3.0 ed., 2021. [Online]. Available: https://www.eurocontrol.int/sites/default/files/2021-07/eurocontrol-tod-manual-ed-3-0.pdf

[6] L. Dong and J. Shan, "A comprehensive review of earthquake-induced building damage detection with remote sensing techniques," *ISPRS J. Photogramm. Remote Sens. 2013*, vol. 84, pp. 85–99, 2013, doi: 10.1016/j.isprsjprs.2013.06.011.

[7] S. Sun and C. Salvaggio, "Aerial 3D building detection and modeling from airborne LiDAR point clouds," *IEEE J. Sel. Topics Appl. Earth Observ. Remote Sens.*, vol. 6, no. 3, pp. 1440–1449, Jun. 2013, doi: 10.1109/JSTARS.2013.2251457.

[8] F. Rottensteiner, G. Sohn, M. Gerke, J. D. Wegner, U. Breitkopf, and J. Jung, "Results of the isprs benchmark on urban object detection and 3D building reconstruction," *ISPRS J. Photogramm. Remote Sens.*, vol. 93, pp. 256–271, 2014, doi: 10.1016/j.isprsjprs.2013.10.004.

[9] I. Colomina and P. Molina, "Unmanned aerial systems for photogrammetry and remote sensing: Areview," *ISPRS J. Photogramm. Remote Sens.*, vol. 92, pp. 79–97, 2014.

[10] R. R. Gamage and H. A. Nalani, "A grid-based automated building extraction technique for low-cost UAV images," *J. Geospatial Surv.*, vol. 1, pp. 23–31, 2021, doi: 10.4038/jgs.v1i1.26.

[11] E. Maltezos and C. Ioannidis, "Automatic detection of building points from lidar and dense image matching point clouds," *ISPRS Ann. Photogramm., Remote Sens. Spatial Inf. Sci.*, vol. II-3/W5, pp. 33–40, 2015, doi: 10.5194/isprsannals-II-3-W5-33-2015.

[12] L. Mitsevich, "3D Aerodrome obstacle assessment using stereo remote sensing imagery," *Int. Arch. Photogramm., Remote Sens. Spatial Inf. Sci.*, vol. XLIII-B2-2020, pp. 1115–1119, 2020.

[13] N. Demir and E. Baltsavias, "Object extraction at airport sites using DTMs/DSMs and multispectral image analysis," international archives of photogrammetry," *Remote Sens. Spatial Inf. Sci.*, vol. 36, pp. 25–30, 2007.

[14] N. Demir, N. Poli, and E. Baltsavias, "Detection of buildings at airport sites using images & LIDAR data and a combination of various methods," *Int. Arch. Photogramm., Remote Sens. Spatial Inf. Sci.*, vol. 38, pp. 71–76, 2009.

[15] C. Parrish and R. Nowak, "Improved approach to LIDAR airport obstruction surveying using full-waveform data," *J. Surv. Eng.*, vol. 135, no. 2, pp. 72–82, 2009.

[16] Y. Xu, S. Tuttas, L. Hoegner, and U. Stilla, "Geometric primitive extraction from point clouds of construction sites using VGS," *IEEE Geosci. Remote. Sens. Lett.*, vol. 14, no. 3, pp. 424–428, Mar. 2017, doi: 10.1109/LGRS.2017.2647816.

[17] Y. Xu, S. Tuttas, L. Heogner, and U. Stilla, "Reconstruction of scaffolds from a photogrammetric point cloud of construction sites using a novel 3D local feature descriptor," *Automat. Construction*, vol. 85, pp. 76–95, 2018.

[18] E. Grilli, F. Menna, and F. Remondino, "A review of point clouds segmentation and classification algorithms," *ISPRS Int. Arch. Photogramm. Remote. Sens. Spatial Inf. Sci.*, vol. XLII-2/W3, pp. 339–344, 2017.

[19] A. Frome, D. Huber, R. Kolluri, T. Bülow, and J. Malik, "Recognising objects in range data using regional point descriptors," in *Proc. 8th Eur.Comput. Vis.*, 2004, pp. 224–237.

[20] M. Rutzinger, B. Höfle, M. Hollaus, and N. Pfeifer, "Object-based point cloud analysis of full-waveform airborne laser scanning data for urban vegetation classification," *Sensors*, vol. 8, no. 8, pp. 4505–4528, 2008.

[21] N. Chehata, L. Guo, and C. Mallet, "Airborne LiDAR feature selection for urban classification using random forests," *Int. Arch. Photogramm. Remote Sens. Spatial Inf. Sci.*, vol. 38, pp. 207–212, 2009.

[22] B. Höfle and M. Hollaus, "Urban vegetation detection using high density full-waveform airborne LiDAR data-combination of object based image and point cloud analysis," in *Proc. ISPRS TC VII Symp. 100 Years ISPRS*, pp. 281–286, 2010.

[23] C. Mallet, F. Bretar, and U. Soergel, "Analysis of full-waveform LiDAR data for classification of urban areas," in *Proc. ISPRS Congr.*, 2008, pp. 337–349.

[24] M. Bassier, B. Van Genechten, and M. Vergauwen, "Classification of sensor independent point cloud data of building objects using random forests," *J. Build. Eng.*, vol. 21, pp. 468–477, 2019.

[25] T. Hackel, J. D. Wegner, and K. Schindler, "Fast semantic segmentation of 3D point clouds with strongly varying density," *ISPRS Ann. Photogramm. Remote Sens. Spatial Inf. Sci.*, vol. 3, pp. 177–184, 2016.

[26] M. Weinmann, B. Jutzi, and C. Mallet, "Feature relevance assessment for the semantic interpretation of 3D point cloud data," *ISPRS Ann. Photogramm. Remote Sens. Spatial Inf. Sci.*, vol. 2, pp. 313–318, 2013.

[27] T. Hackel, N. Savinov, L. Ladicky, J. D. Wegner, K. Schindler, and M. Pollefeys, "Semantic3D net: A new large-scale point cloud classification benchmark," *ISPRS Ann. Photogramm. Remote Sens. Spatial Inf. Sci.*, vol. 4, pp. 91–98, 2017.

[28] J. Zhang, X. Lin, and X. Ning, "SVM-based classification of segmented airborne LiDAR point clouds in urban areas," *Remote Sens.,* vol. 5, no. 8, pp. 3749–3775, 2013.

[29] B. Jutzi and H. Gross, "Nearest neighbour classification on laser point clouds to gain object structures from buildings," *Int. Arch. Photogramm. Remote Sens. Spatial Inf. Sci.*, vol. 38, pp. 4–7, 2009.

[30] C. R. Qi, H. Su, K. Mo, and L. J. Guibas, "Pointnet: Deep learning on point sets for 3D classification and segmentation," in *Proc. IEEE Conf. Comput. Vis. Pattern Recognit.*, 2017, pp. 652–660, doi: 10.1109/CVPR.2017.16.

[31] A. Bab-Hadiashar and N. Gheissari, "Range image segmentation using surface selection criterion," *IEEE Trans. Image Process.*, vol. 15, no. 7, pp. 2006–2018, 2006, doi: 10.1109/TIP.2006.877064.

[32] A. Aldoma *et al.*, "Tutorial: Point cloud library: Three-dimensional object recognition and 6 dof pose estimation," *IEEE Robot. Autom. Mag.*, vol. 19, no. 3, pp. 80–91, Sep. 2012, doi: 10.1109/mra.2012.2206675.

[33] X. Lu, J. Yao, J. Tu, K. Li, L. Li, and Y. Liu, "Pairwise linkage for point cloud segmentation," *ISPRS Ann. Photogramm. Remote. Sens. Spatial. Inf. Sci.*, vol. III-3, pp. 201–208, 2016.
[34] H. Aljumaily, D. F. Laefer, and D. Cuadra, "Urban point cloud mining based on density clustering and mapreduce," *J. Comput. Civil Eng.*, vol. 31, 2017, Art. no. 04017021.
[35] A. V. Vo, L. Truong-Hong, D. F. Laefer, and M. Bertolotto, " Octree-based region growing for point cloud segmentation," *ISPRS J. Photogramm. Remote. Sens.*, vol. 104, pp. 88–100, 2015.
[36] D. Tóvári and N. Pfeifer, "Segmentation based robust interpolation-a new approach to laser data filtering," *ISPRS Int. Arch. Photogramm. Remote. Sens. Spat. Inf. Sci.*, vol. 36, pp. 79–84, 2005.
[37] T. Rabbani, F. Van Den Heuvel, and G. Vosselmann, "Segmentation of point clouds using smoothness constraint," *ISPRS Int. Arch. Photogramm. Remote. Sens. Spat. Inf. Sci.*, vol. 36, pp. 248–253, 2006.
[38] P. Besl and R. Jain, "Segmentation through variable-order surface fitting," *IEEE Trans. Pattern Anal. Mach. Intell.*, vol. 10, no. 2, pp. 167–192, Mar. 1988, doi: 10.1109/34.3881.
[39] A. Nurunnabi, D. Belton, and G. West, "Robust segmentation for large volumes of laser scanning three-dimensional point cloud data," *IEEE Trans. Geosci. Remote. Sens.*, vol. 54, no. 8, pp. 4790–4805, Aug. 2016.
[40] P. Dorniger and N. Pfeifer, "A comprehensive automated 3D approach for building extraction, re construction and regularisation from air borne laser scanning point cloud," *Sensors*, vol. 8, pp. 7323–7343, 2008.
[41] A. Nguyen and B. Le, "3D point cloud segmentation: A survey," in *Proc. 6th Conf. Robot., Automat. Mechatronics*, Nov. 2013, pp. 225–230.
[42] R. Schnabel, R. Wahl, and R. Klein, "Efficient RANSAC for point-cloud shape detection," *Comput. Graph. Forum*, vol. 26, pp. 214–226, 2007.
[43] J. Bauer, K. Karner, K. Schindler, A. Klaus, and C. Zach, "Segmentation of building from dense 3D point-clouds," in *Proc. 27th Workshop Austrian Assoc. Pattern Recognit.*, 2005, pp. 253–259.
[44] H. Boulaassal, "Segmentation et modélisation géométrique de façades de bâtiments à partir de relevés laser terrestres," Ph.D. Thesis, Université de Strasbourg, Strasbourg, France, 2010.
[45] T. M. Awwad, Q. Zhu, Z. Du, and Y. Zhan, "An improved segmentation approach for planar surfaces from unstructured 3D point clouds," *Photogramm. Rec.*, vol. 25, no. 129, pp. 5–23, 2010.
[46] J. A. Delmerico, P. David, and J. J. Corso, "Building facade detection, segmentation, and parameter estimation for mobile robot localization and guidance," in *Proc. Int. Conf. Intell. Robots Syst.*, 2011, doi: 10.1109/IROS.2011.6094778.
[47] M. Y. Yang and W. Forstner, "Plane detection in point cloud data," 2010. [Online]. Available: https://ris.utwente.nl/ws/files/103953896/Yang2010Plane.pdf
[48] J.-E. Deschaud, "Traitements de nuages de points denses et modélisation 3D d'environnement par système mobile LIDAR/Caméra," Ph.D. Thesis, MINES ParisTech, Paris, France.
[49] S. Tuttas and U. Stilla, "Window detection in sparse point clouds using indoor points," international archives of photogrammetry," *Remote Sens. Spatial Inf. Sci.*, vol. 38, no. 3/W22, pp. 131–136, 2011.
[50] M. Jarząbek-Rychard and A. Borkowski, "Porównanie algorytmów RANSAC oraz rosnących płaszczyzn w procesie segmentacji danych z lotniczego skaningu laserowego," (in Polish), *Archiwum Fotogrametrii, Kartografii i Teledetecji*, vol. 21, pp. 119–129, 2010.
[51] F. Tarsha Kurdi, "Extraction et reconstruction de bâtiments en 3D à partir de relevés lidar aéroportés," Ph.D. Thesis, Université de Strasbourg, Strasbourg, France, 2008.
[52] Z. Rozsa and T. Sziranyi, "Obstacle prediction for automated guided vehicles based on point clouds measured by a tilted LIDAR sensor," *IEEE Trans. Intell. Transp. Syst.*, vol. 19, no. 8, pp. 2708–2720, Aug. 2018, doi: 10.1109/TITS.2018.2790264.
[53] Y. Choe, S. Ahn, and M. J. Chung, "Online urban object recognition in point clouds using consecutive point information for urban robotic missions," *Robot. Auton. Syst.*, vol. 62, no. 8, pp. 1130–1152, 2014, doi: 10.1016/j.robot.2014.04.007.
[54] M. Hammer, M. Hebel, M. Laurenzis, and M. Arens, "Lidar-based detection and tracking of small UAVs," *Proc. SPIE*, 2018, vol. 10799, Art. no. 107990S.
[55] P. Wu, S. Xie, H. Liu, J. Luo, and Q. Li, "A novel algorithm of autonomous obstacle-avoidance for mobile robot based on LIDAR data," in *Proc. IEEE Int. Conf. Robot. Biomimetics*, 2015, pp. 2377–2382.
[56] Annex 15 to the Convention on International Civil Aviation, "International standards and recommended practices," Aeronautical Information Services, ICAO, 15ed., 2016. [Online]. Available: https://ffac.ch/wp-content/uploads/2020/10/ICAO-Annex-15-Aeronautical-Information-Services.pdf
[57] Annex 4 to the Convention on International Civil Aviation, "Aeronautical charts," ICAO, 11ed., 2009. [Online]. Available: https://aviation-is.better-than.tv/icaodocs/Annex%204%20-%20Aeronautical%20Charts/Annex%204%20Aeronautical%20Charts,%20Edition%20no%2011.pdf
[58] DOC-9674, "World geodetic system-1984 (WGS84) manual," ICAO, 2ed., 2002. [Online]. Available: https://skybrary.aero/sites/default/files/bookshelf/5854.pdf
[59] DOC-1006, Aeronautical informationmanagement, ICAO, 1ed., 2018. [Online]. Available: https://ffac.ch/wp-content/uploads/2020/11/ICAO-Doc-10066-Aeronautical-Information-Management.pdf
[60] "Rozporządzenie ministra infrastruktury z dnia 12 stycznia 2021 r. w sprawie przeszkód lotniczych, powierzchni ograniczających przeszkody oraz urządzeń o charakterze niebezpiecznym," Dziennik Ustaw, 2021, poz. 264., in Polish. [Online]. Available: https://isap.sejm.gov.pl/isap.nsf/DocDetails.xsp?id=WDU20210000264
[61] M. A. Fischler and R. C. Bolles, "Random sample consensus: A paradigm for model fitting with applications to image analysis and automated cartography," *Commun. ACM*, vol. 24, no. 6, pp. 381–395, 1981.
[62] M. Zuliani, "RANSAC for dummies," Los Gatos, pp. 8–93, 2012. [Online]. Available: https://www.ic.unicamp.br/∗sim;rocha/teaching/2012s1/mc949/aulas/ransac-4-dummies.pdf
[63] G. Vosselman, B. G. H. Gorte, G. Sithole, and T. Rabbani, "Recognising structure in laser scanner point clouds," *Int. Arch. Photogramm., Remote Sens. Spatial Inf. Sci.*, vol. 36, pp. 33–38, 2004.
[64] M. Zuliani, RANSAC, 2009. [Online]. Available: http://vision.ece.ucsb.edu/∼zuliani/Research/RANSAC/docs/
[65] M. Rogowski and J. A. Prusiel, "Budynek wysokościowy," (in Polish), Przegląd Budowlany, Warsaw, Poland, 2019.
[66] W. Dominik, "Comparison of point clouds derived from aerial image matching with data from airborne laser scanning," *Archiwum Fotogrametrii, Kartografii i Teledetekcji*, vol. 26, pp. 53–66, 2014.
[67] L. Wallace, A. Lucieer, Z. Malenovský, D. Turner, and P. Vopěnka, "Assessment of forest structure using two UAV techniques: A comparison of airborne laser scanning and structure from motion (SfM) point clouds," *Forests*, vol. 7, no. 3, pp. 1–16, 2016.
[68] T. Gobakken, O. M. Bollandsås, and E. Næsset, "Comparing biophysical forest characteristics estimated from photogrammetric matching of aerial images and airborne laser scanning data," *Scand. J. Forest Res.*, vol. 30, pp. 73–86, 2015.
[69] S. Puliti, T. Gobakken, H. O. Ørka, and E. Næsset, "Assessing 3D point clouds from aerial photographs for species-specific forest inventories," *Scand. J. Forest Res.*, vol. 32, pp. 68–79, 2017.
[70] S. Tuominen, A. Balazs, H. Saari, I. Pölönen, J. Sarkeala, and R. Viitala, "Unmanned aerial system imagery and photogrammetric canopy height data in area-based estimation of forest variables," *Silva Fennica*, vol. 49, 2015, Art. no. 1348.

Marta Lalak received the M.Sc. degree in geoinformatics from Military University of Technology, Warsaw, Poland, in 2010. She is currently working toward the Ph.D. degree in engineering and technical sciences from Polish Air Force University.

She is a Lecturer with the Institute of Navigation of the Military University of Aviation, where she conducts classes on "GIS in navigation," "basics of photogrammetry," "basics of remote sensing," "image recognition." Her research interests include UAV-acquired data processing and aviation obstacle detection. He was with the Department of Imagery Intelligence, Faculty of Civil Engineering and Geodesy, Military University of Technology, Warsaw, Poland.

Damian Wierzbicki received the Ph.D degree in photogrammetry and remote sensing from Military University of Technology, Warsaw, Poland, in 2015.

He is currently an Associate Professor with the Department of Imagery Intelligence, Faculty of Civil Engineering and Geodesy, Military University of Technology where he teaches: "Photogrammetry and Remote Sensing" and "Image Processing." His research interests include UAV navigation and image processing, deep learning in remote sensing. His research interests also include development of new algorithms for object detection and classification in image sequences from UAV.